Analytical Methods

DOI: 10.1002/anie.201207348

Metabolic Differences in Microbial Cell Populations Revealed by Nanophotonic Ionization**

*Bennett N. Walker, Cory Antonakos, Scott T. Retterer, and Akos Vertes**

Growing interest in functional genomics[1] has resulted in technological breakthroughs in advanced proteomics, including the intracellular microproteomic analysis of tissues and cells.[2] Quantitative differences in the proteome at the single-cell level can be detected by flow cytometry and fluorescence,[3] as well as mass spectrometry,[4,5] whereas microbial single cell metabolomics has not progressed as rapidly because it involves studying compounds of larger chemical variety, higher turnover rates, and lower molecular weights, coincident with the mass range of common contaminants. Owing to the low copy number of some intracellular proteins and the presence of extracellular noise, isogenic cells can exhibit large differences in their metabolic makeup.[6] This metabolic noise, part of cellular differences, is poorly characterized because it requires the multicomponent analysis of severely volume-limited samples, that is, individual microbial cells. A technique that can capture metabolic variations for a large fraction of the hundreds to thousands of metabolites in single cells or small populations requires a combination of ultra-low limits of detection, high selectivity, and high quantitation capability.[7–9]

Currently, most metabolic studies are conducted using fluorescence measurements,[10] NMR spectroscopy,[11,12] or mass spectrometry (MS).[8,13–18] Fluorescence measurements provide an ultra-low limit of detection and high selectivity[10] but typically require labeling of selected metabolites, making the process laborious, time consuming, and potentially invasive. NMR and MS are often considered to be complementary techniques; NMR is viewed as a universal detector that does not rely on separation but lacks the sensitivity to analyze single cells. Mass spectrometry is a highly sensitive technique, but to achieve sufficient selectivity and peak capacity, it is often coupled with separation techniques. LC–MS[19] and GC–MS[20–23] are efficient methods to detect and quantitate thousands of metabolites in complex extracts from large cell populations. These methods require thousands to millions of cells to achieve a high coverage of the metabolome. The analysis of cellular metabolites using secondary ion MS (SIMS),[24,25] MALDI MS,[16,26] and laser desorption ionization (LDI) on nanoporous structures[8] shows promise for large-scale metabolomic studies.

Recently, we introduced silicon nanopost arrays (NAPA) as a matrix-free LDI-MS method with highly enhanced ion yields and photonic properties.[27–29] A typical NAPA chip is comprised of over two million ordered monolithic silicon nanoposts (see inset in Figure 1 b). The array is defined by the height, H, diameter, D, and periodicity, P, of the posts. Posts of a given diameter exhibit an ion yield resonance at a particular aspect ratio (Supporting Information, Figure S1).

In this study, *Saccharomyces cerevisiae* was chosen for exploring the metabolome in small cell populations and single cells, because the yeast metabolome and metabolic networks are relatively small and have been extensively analyzed.[30] Without distinguishing chemical species in the different cellular compartments, there are 584 known metabolites that take part in 1175 reactions organized into 94 major biochemical pathways.[31] We demonstrate that LDI from NAPA can capture metabolic changes in single yeast cells and small cell populations owing to oxidative stress. Intra- and inter-population differences can also be examined by this method.

AFM imaging of a yeast cell on a NAPA before and after laser exposure showed that, as a consequence of the laser radiation, the intracellular contents were released onto the nanostructure (Figure 1 a). Our results indicate that the limit of detection for the LDI of various organic and biomolecules from NAPA can reach approximately 800 zeptomoles (measured for verapamil standards).[33] Because the estimated amounts of some primary metabolites, for example, amino acids, in an approximately 30 fL yeast cell are in the 10 amol to 30 fmol range, the sensitivity of the NAPA technique should be sufficient for single microbial-cell analysis.

Small populations ($1 \le n \le 80$) of *S. cerevisiae* were directly deposited and analyzed on NAPA. In the mass range of small metabolites (50–500 Da), the mass spectra generated by LDI resulted in numerous peaks yielding up to 108 assignments (Figure 1 b) that corresponded to 18 % of the known metabolome. Table S1 (Supporting Information) shows the list of metabolite assignments derived from LDI-MS using NAPA. These tentative assignments were curated from multiple datasets, assuming protonation and addition of Na^+ or K^+ ions in the positive ion mode, as well as proton loss

[*] Dr. B. N. Walker, C. Antonakos, Prof. A. Vertes
Department of Chemistry, The George Washington University
Washington, DC 20052 (USA)
E-mail: vertes@gwu.edu
Homepage: http://www.gwu.edu/~vertes
Dr. S. T. Retterer
Oak Ridge National Laboratory
Oak Ridge, TN 37831 (USA)

[**] Support from the Division of Chemical Sciences, Geosciences, and Biosciences, Office of Basic Energy Sciences of the U.S. Department of Energy (Grant DE-FG02-01ER15129) is gratefully acknowledged. A portion of this research (nanofabrication) was conducted at the Center for Nanophase Materials Sciences, which is sponsored at Oak Ridge National Laboratory by the Scientific User Facilities Division, Office of Basic Energy Sciences, U.S. Department of Energy.

Supporting information for this article is available on the WWW under http://dx.doi.org/10.1002/anie.201207348.

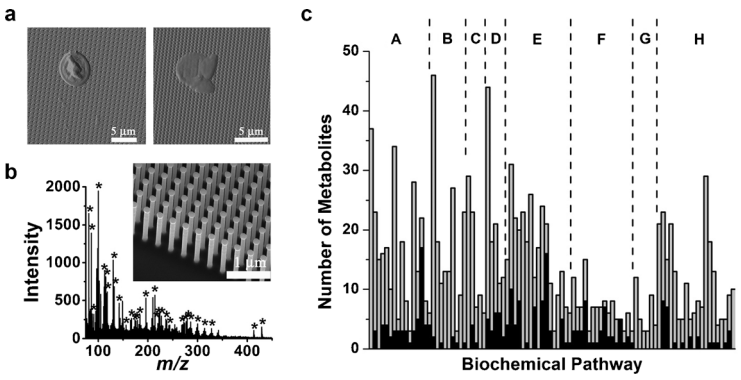

Figure 1. a) AFM images of a single *S. cerevisiae* cell on NAPA before (left) and after (right) laser exposure. As the cell wall is ruptured by the laser pulse, the intracellular metabolites are exposed and ionization occurs. b) Laser irradiation of 78 yeast cells on the NAPA (* = identified metabolite). Inset: SEM image of the NAPA used herein. c) Bar graph comparing the number of metabolites involved in particular biochemical pathways (gray) to the number of identified metabolites (black). The major biochemical pathways are as follows: A) amino acid biosynthesis, B) fatty acid and lipid biosynthesis, C) carbohydrate biosynthesis, D) nucleoside/tide biosynthesis, E) biosynthesis of cofactors, prosthetic groups, and electron carriers, F) amino acid degradation, G) carbohydrate and sugar degradation, and H) all other biochemical pathways, including the TCA cycle.

for the formation of negative ions. The assignments were based on mass accuracy with a $\Delta m/z \leq 0.06$ cutoff from metabolite searches in the *Saccharomyces* Genome Database (SGD) (http://www.yeastgenome.org/). Further validation of most of the assignments requires tandem MS and functional studies.

Based on these LDI-MS measurements, Figure 1c shows the coverage of individual metabolic pathways grouped into families. Table S2 summarizes the aggregated metabolite coverage for families of biochemical pathways and super-pathways. The metabolite coverage was calculated as a percentage of the total number of metabolites in the pathway family. Two additional examples of high-metabolite coverage are shown in Figure S2 for the super-pathway for threonine and methionine biosynthesis, and the super-pathway for the tricarboxylic acid (TCA) cycle and the glyoxylate cycle. Counting the pathways that had at least one metabolite assigned in the spectra, 67% coverage of the 94 major pathways was established (see Figure S2 for the coverage of two selected biochemical pathways).

As metabolite turnover rates in microorganisms are faster than changes observed in the genome and the proteome, intracellular metabolic content can be sensitive to analysis conditions. In addition, significant metabolic differences can be expected within and among cell populations.[32] Therefore, analyzing the variances between the spectra of individual cells, rather than the large populations required for LC–MS[19] and GC–MS,[20] can reveal intra- and inter-population differences.

Separation and analysis techniques for single animal cells have recently been introduced and are currently used in various research laboratories.[9,10] These metabolic studies involve either the analysis of only a few chemical species using fluorescence, or require the use of larger cells with volumes of 500 fL or greater. NAPA has the sensitivity and quantitation capabilities (Figure S3) to enable the analysis of single yeast cells with approximately 30 fL volume for multiple metabolites.[33] Figure 2a shows the LDI mass spectrum of a single yeast cell deposited onto the NAPA surface with minimal interference from background ions. The identified peaks correspond to up to 24 species or up to 4% of the known metabolome with at least one metabolite detected from 29% of the major biochemical pathways. The pathways with the highest coverage were the biosynthesis of amino acids, nucleotides, and cofactors. Minimal background interference and multispecies coverage represent promising attributes for this label-free single-cell analysis method.

Ion abundance changes in NAPA spectra enable the quantitative metabolic analysis of small cell populations and single cells. Comparing the spectra for cell population sizes of $n = 1$ and 79 in Figure 2a,b, respectively, indicates more abundant peaks from a larger number of species in the multicell spectrum. By plotting ion intensities for four common amino acids (proline, lysine, methionine, and cysteine) as a function of absolute amounts

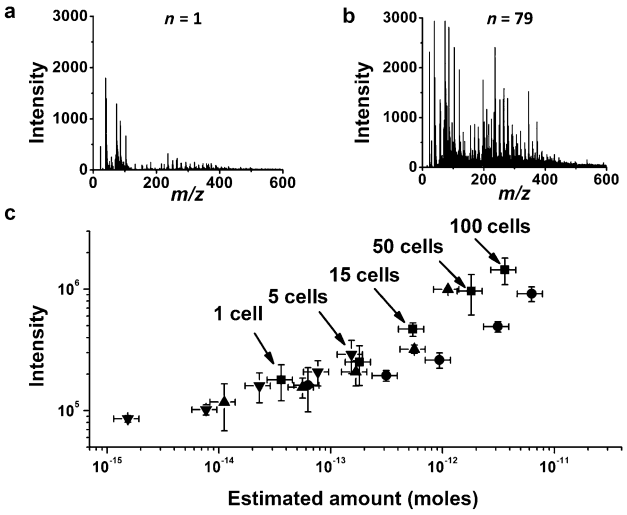

Figure 2. a) Mass spectrum of a single *S. cerevisiae* cell by LDI-MS from NAPA. b) Mass spectrum from 79 yeast cells by LDI-MS from NAPA. c) Ion intensities for four amino acids (proline (■), lysine (●), methionine (▲), and cysteine (▼)) as a function of their estimated amounts in small cell populations of increasing size in the $1 \leq n \leq 100$ range. Cell numbers are indicated for proline. The calculated volume of a cell is approximately 30 fL.

estimated for population sizes between $n = 1$ and $n = 100$ from the average biomass composition of *S. cerevisiae*,[31] a quantitative response can be established and analyzed with a dynamic range of up to three orders of magnitude.

Metabolic network reconstruction of *S. cerevisiae* based on genomic information[34] and flux balance analysis can be used to determine the essential reactions, the participating biochemical species, and predict complex intracellular changes that are due to environmental stimuli.[31] Multiple

attempts to establish the metabolic network for *S. cerevisiae* have led to the emergence of consensus models.[35] As the metabolic map is both complex and can undergo functional changes, rapid multispecies verification of the models is necessary. The direct analysis of numerous intracellular yeast metabolites in conjunction with quantitation capabilities, demonstrated in Figure 2c, can be used to verify these models and perhaps resolve ambiguities.

To observe the physiological response in small microbial cell populations, we studied the metabolic changes in *S. cerevisiae* under oxidative stress induced by hydrogen peroxide in the growth medium. Small populations ($n < 80$) of stressed and control cells were studied by LDI-MS from NAPA to determine the up- and downregulation of various metabolites. Orthogonal projections to latent structures discriminant analysis (OPLS-DA) of the spectra indicated that the observed differences between the stressed and control populations were statistically significant.

Studying oxidative stress in small yeast cell populations indicated a metabolic response that resulted in significantly changed metabolite levels (Figure 3; Table S3). To identify the metabolites responsible for most of the variance between the spectra from the stressed and control cell populations, S-plots were constructed. For metabolites corresponding to the points with both high correlation and covariance values (the "wings" of the curve), paired-sample t-tests were conducted with a $p < 0.05$ cutoff to assess if the ion intensity changes were statistically significant. In populations of $n \approx 80$ yeast cells exposed to oxidative stress, 21 statistically significant metabolic changes were identified. An additional ten peaks in the mass spectra showed significant changes, but they remained unassigned.

In the stressed populations, the upregulation of glutathione (a major intracellular redox buffer known to curb oxidative damage) was observed ($p < 0.002$), along with two metabolites involved in its biosynthesis, cysteinylglycine and glutamylcysteine. Although the upregulation of urate, an alternative redox buffer, was also observed, *S. cerevisiae* does not have the gene for urate oxidase (UOX), the enzyme necessary for it to curb hydrogen peroxide.[36] Downregulation of compounds related to folate biosynthesis, responsible for promoting cellular growth, such as amino-4-deoxychorismate and dihydroneopterin phosphate, were also observed ($p < 4 \times 10^{-4}$) indicating that the cells redirected resources from growth to fighting stress.

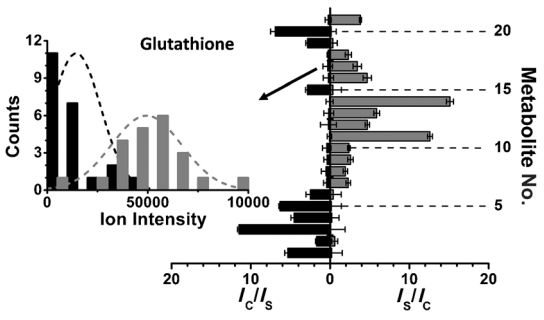

Figure 3. Upregulation of 12 intracellular metabolites (gray bars, right axis) was observed after cells ($n \approx 80$) were exposed to oxidative stress for one hour. Downregulation was seen for another nine intracellular metabolites (black bars, left axis). Inset: histogram of the ion intensity distributions for glutathione with (gray) or without (black) oxidative stress. The shift in the mean of the distribution indicates the inter-population differences.

Comparing the single cell spectra from the two populations (see Figure S4a,b for an example of each) by OPLS-DA indicated clear clustering (Figure S4c) and the absence of strong outliers. The analysis showed that the spectra from the stressed and control groups were well separated even at the single cell level (see the scores plot and the S-plot in Figure S4 and Figure S5a, respectively).

To identify the metabolites responsible for most of the variance between the single cell spectra of the stressed and control populations, an S-plot was generated (Figure S5a). Inspecting the points with high covariance and correlation revealed that threonine and sedoheptulose phosphate were upregulated, whereas dimethylsulfide, proline, and glycerol phosphate were downregulated. These and other compounds with similar parameters in the S-plot can be regarded as putative biomarkers for oxidative stress derived from single-cell studies. The differences in the ion intensity distributions for threonine and dimethylsulfide are apparent from the histograms in Figure S5b,c. Paired-sample t-tests on this data confirmed that these changes were statistically significant with $p < 6 \times 10^{-5}$ for threonine and $p < 4 \times 10^{-5}$ for dimethylsulfide. These examples demonstrate that cellular differences can be captured by single cell analysis using LDI-MS from the NAPA ionization method.

To determine the distributions of the measured ion intensities, spectra from 20 single cells were acquired (Figure S3a). Histograms of the distributions of the relative ion intensities for leucine and serine are shown Figure S3b. Standard deviations of the average ion intensities, derived from the single cell spectra, were used to assess cellular differences. To separate the intra-population differences from the method-related fluctuations, the variance of the latter was determined on standard solution samples representing analyte amounts similar to what was contained in a single cell. The variance of the method was then subtracted from the measured variance to yield the variance owing to cellular differences. Relative standard deviations for the intra-population cellular differences of lysine, methionine, cysteine, and proline were 26%, 30%, 10% and 25%, respectively. Based on the histograms, there were no subpopulations with separate mean averages.

Quantitative investigation of the cellular differences for various metabolites at the single-cell level can aid in the analysis of metabolic noise.[37,38] The histogram in the inset of Figure 3 shows how the ion intensity distribution for glutathione changes as a result of oxidative stress. The shift in the mean of the distribution indicates the inter-population differences. Intra-population differences can be derived from single-cell studies. Figure S5b,c shows the distribution of threonine and dimethylsulfide ion intensities. The widths of the distributions are linked to the intra-population differences, whereas the difference in the means indicate inter-population differences.

Currently, information about microbial physiology is obtained in large cell populations (approximately 106 cells)

through the observation of a single or a few predetermined metabolic markers and/or through labeling.[39] Nanofabrication of NAPA structures enables tailoring of the critical nanopost parameters to best suit the analysis of particular microorganisms and also to potentially separate and lyse the cells. Using LDI-MS on NAPA allows for multispecies analysis of metabolites without their isolation or the use of labels.[40] As a result, a more complete and rapid assessment of cellular responses to external and pathophysiological stresses, normal functional changes, or various mutations[41] can be observed in small ($1 < n \leq 100$) cell populations or using single cells.

The combination of direct cellular analysis on NAPA and metabolic network modeling on small populations will enhance our understanding of the roles of metabolic noise and provide needed insight into functional changes, as well as intracellular responses, to external and pathophysiological stresses. Further research is needed to broaden the coverage of the metabolome, including the metabolites involved in the biosynthesis of carbohydrates.

Received: September 12, 2012
Revised: December 19, 2012
Published online: February 27, 2013

Keywords: cellular differences · mass spectrometry · metabolites · nanostructures · single-cell analysis

[1] G. A. Evans, *Nat. Biotechnol.* **2000**, *18*, 127.
[2] H. B. Gutstein, J. S. MorriS, S. P. Annangudi, J. V. Sweedler, *Mass Spectrom. Rev.* **2008**, *27*, 316 – 330.
[3] J. R. S. Newman, S. Ghaemmaghami, J. Ihmels, D. K. Breslow, M. Noble, J. L. DeRisi, J. S. Weissman, *Nature* **2006**, *441*, 840 – 846.
[4] D. R. Bandura, V. I. Baranov, O. I. Ornatsky, A. Antonov, R. Kinach, X. D. Lou, S. Pavlov, S. Vorobiev, J. E. Dick, S. D. Tanner, *Anal. Chem.* **2009**, *81*, 6813 – 6822.
[5] S. C. Bendall, E. F. Simonds, P. Qiu, E. A. D. Amir, P. O. Krutzik, R. Finck, R. V. Bruggner, R. Melamed, A. Trejo, O. I. Ornatsky, R. S. Balderas, S. K. Plevritis, K. Sachs, D. Pe'er, S. D. Tanner, G. P. Nolan, *Science* **2011**, *332*, 687 – 696.
[6] C. V. Rao, D. M. Wolf, A. P. Arkin, *Nature* **2002**, *420*, 231 – 237.
[7] A. Amantonico, J. Y. Oh, J. Sobek, M. Heinemann, R. Zenobi, *Angew. Chem.* **2008**, *120*, 5462 – 5465; *Angew. Chem. Int. Ed.* **2008**, *47*, 5382 – 5385.
[8] T. R. Northen, O. Yanes, M. T. Northen, D. Marrinucci, W. Uritboonthai, J. Apon, S. L. Golledge, A. Nordstrom, G. Siuzdak, *Nature* **2007**, *449*, 1033 – 1036.
[9] S. S. Rubakhin, E. V. Romanova, P. Nemes, J. V. Sweedler, *Nat. Methods* **2011**, *8*, S20 – S29.
[10] C. E. Sims, N. L. Allbritton, *Lab Chip* **2007**, *7*, 423 – 440.
[11] J. L. Griffin, *Philos. Trans. R. Soc. London Ser. B* **2004**, *359*, 857 – 871.
[12] S. Moco, B. Schneider, J. Vervoort, *J. Proteome Res.* **2009**, *8*, 1694 – 1703.
[13] J. I. Castrillo, A. Hayes, S. Mohammed, S. J. Gaskell, S. G. Oliver, *Phytochemistry* **2003**, *62*, 929 – 937.
[14] J. Højer-Pedersen, J. Smedsgaard, J. Nielsen, *Metabolomics* **2008**, *4*, 393 – 405.
[15] L. J. Li, R. W. Garden, J. V. Sweedler, *Trends Biotechnol.* **2000**, *18*, 151 – 160.
[16] A. Amantonico, P. L. Urban, S. R. Fagerer, R. M. Balabin, R. Zenobi, *Anal. Chem.* **2010**, *82*, 7394 – 7400.
[17] B. Shrestha, A. Vertes, *Anal. Chem.* **2009**, *81*, 8265 – 8271.
[18] L. Wu, M. R. Mashego, J. C. van Dam, A. M. Proell, J. L. Vinke, C. Ras, W. A. van Winden, W. M. van Gulik, J. J. Heijnen, *Anal. Biochem.* **2005**, *336*, 164 – 171.
[19] Y. F. Shen, R. Zhang, R. J. Moore, J. Kim, T. O. Metz, K. K. Hixson, R. Zhao, E. A. Livesay, H. R. Udseth, R. D. Smith, *Anal. Chem.* **2005**, *77*, 3090 – 3100.
[20] S. G. Villas-Bôas, J. F. Moxley, M. Akesson, G. Stephanopoulos, J. Nielsen, *Biochem. J.* **2005**, *388*, 669 – 677.
[21] S. G. Villas-Bôas, J. Hojer-Pedersen, M. Akesson, J. Smedsgaard, J. Nielsen, *Yeast* **2005**, *22*, 1155 – 1169.
[22] J. Smedsgaard, J. Nielsen, *J. Exp. Bot.* **2005**, *56*, 273 – 286.
[23] K. F. Smart, R. B. M. Aggio, J. R. Van Houtte, S. G. Villas-Boas, *Nat. Protoc.* **2010**, *5*, 1709 – 1729.
[24] S. G. Ostrowski, C. T. Van Bell, N. Winograd, A. G. Ewing, *Science* **2004**, *305*, 71 – 73.
[25] M. E. Kurczy, P. D. Piehowski, C. T. Van Bell, M. L. Heien, N. Winograd, A. G. Ewing, *Proc. Natl. Acad. Sci. USA* **2010**, *107*, 2751 – 2756.
[26] G. Sun, K. Yang, Z. D. Zhao, S. P. Guan, X. L. Han, R. W. Gross, *Anal. Chem.* **2007**, *79*, 6629 – 6640.
[27] B. N. Walker, J. A. Stolee, D. L. Pickel, S. T. Retterer, A. Vertes, *J. Phys. Chem. C* **2010**, *114*, 4835 – 4840.
[28] B. N. Walker, T. Razunguzwa, M. Powell, R. Knochenmuss, A. Vertes, *Angew. Chem.* **2009**, *121*, 1697 – 1700; *Angew. Chem. Int. Ed.* **2009**, *48*, 1669 – 1672.
[29] J. A. Stolee, B. N. Walker, V. Zorba, R. E. Russo, A. Vertes, *Phys. Chem. Chem. Phys.* **2012**, *14*, 8453 – 8471.
[30] S. P. Gygi, B. Rist, S. A. Gerber, F. Turecek, M. H. Gelb, R. Aebersold, *Nat. Biotechnol.* **1999**, *17*, 994 – 999.
[31] J. Forster, I. Famili, P. Fu, B. O. Palsson, J. Nielsen, *Genome Res.* **2003**, *13*, 244 – 253.
[32] O. Fiehn, *Plant Mol. Biol.* **2002**, *48*, 155 – 171.
[33] B. N. Walker, J. A. Stolee, A. Vertes, *Anal. Chem.* **2012**, *84*, 7756 – 7762.
[34] A. Goffeau, B. G. Barrell, H. Bussey, R. W. Davis, B. Dujon, H. Feldmann, F. Galibert, J. D. Hoheisel, C. Jacq, M. Johnston, E. J. Louis, H. W. Mewes, Y. Murakami, P. Philippsen, H. Tettelin, S. G. Oliver, *Science* **1996**, *274*, 546 – 567.
[35] M. J. Herrgård, N. Swainston, P. Dobson, W. B. Dunn, K. Y. Arga, M. Arvas, N. Bluthgen, S. Borger, R. Costenoble, M. Heinemann, M. Hucka, N. Le Novere, P. Li, W. Liebermeister, M. L. Mo, A. P. Oliveira, D. Petranovic, S. Pettifer, E. Simeonidis, K. Smallbone, I. Spasic, D. Weichart, R. Brent, D. S. Broomhead, H. V. Westerhoff, B. Kirdar, M. Penttila, E. Klipp, B. O. Palsson, U. Sauer, S. G. Oliver, P. Mendes, J. Nielsen, D. B. Kell, *Nat. Biotechnol.* **2008**, *26*, 1155 – 1160.
[36] S. Wong, K. H. Wolfe, *Nat. Genet.* **2005**, *37*, 777 – 782.
[37] F. J. Bruggeman, N. Bluthgen, H. V. Westerhoff, *PLoS Comput. Biol.* **2009**, *5*, e1000506.
[38] G. Balázsi, A. van Oudenaarden, J. J. Collins, *Cell* **2011**, *144*, 910 – 925.
[39] M. G. Wiebe, E. Rintala, A. Tamminen, H. Simolin, L. Salusjarvi, M. Toivari, J. T. Kokkonen, J. Kiuru, R. A. Ketola, P. Jouhten, A. Huuskonen, H. Maaheimo, L. Ruohonen, M. Penttila, *FEMS Yeast Res.* **2008**, *8*, 140 – 154.
[40] M. R. Mashego, K. Rumbold, M. De Mey, E. Vandamme, W. Soetaert, J. J. Heijnen, *Biotechnol. Lett.* **2007**, *29*, 1 – 16.
[41] L. M. Raamsdonk, B. Teusink, D. Broadhurst, N. S. Zhang, A. Hayes, M. C. Walsh, J. A. Berden, K. M. Brindle, D. B. Kell, J. J. Rowland, H. V. Westerhoff, K. van Dam, S. G. Oliver, *Nat. Biotechnol.* **2001**, *19*, 45 – 50.

Angewandte Chemie
Eine Zeitschrift der Gesellschaft Deutscher Chemiker

Supporting Information

69451 Weinheim, Germany

Metabolic Differences in Microbial Cell Populations Revealed by Nanophotonic Ionization**

*Bennett N. Walker, Cory Antonakos, Scott T. Retterer, and Akos Vertes**

anie_201207348_sm_miscellaneous_information.pdf

Cellular differences are linked to cell differentiation, the proliferation of cancer and to the development of drug resistance in microbial infections. Due to sensitivity limitations, however, large-scale metabolic analysis at the single cell level is only available for cells significantly larger in volume than *Saccharomyces cerevisiae* (~30 fL). Here we demonstrate that by a nanophotonic ionization platform and mass spectrometry, up to 108 metabolites, or up to 18% of the known *S. cerevisiae* metabolome, can be identified in very small cell populations ($n < 100$). Relative quantitation of up to 4% of the metabolites is achieved at the single cell level. The identified metabolites belong to 63 of the 94 common metabolic pathways with most of them present in amino acid, carbohydrate, nucleotide and lipid biosynthesis and degradation. Following the changes in metabolic states under oxidative stress reveals inter-population differences, i.e., a significant upregulation ($p < 0.002$) of the redox buffer glutathione and the related cysteinylglycine and glutamylcysteine. Downregulation ($p < 4\times10^{-4}$) of amino-deoxychorismate and dihydroneopterin phosphate, used in folate biosynthesis, as well as of oxalureate indicates that the cell redirects resources from cell growth toward fighting oxidative stress. Single cell analyses show that relative standard deviations due to intra-population differences for the abundance of lysine, methionine, cysteine, and proline, in the unperturbed yeast population are 26%, 30%, 10% and 25%, respectively. Enabling large-scale metabolomic studies of single yeast cells opens the door to following functional changes in evolving heterogeneous microbial populations and the analysis of metabolic noise across a cell population.

Materials and Methods

NAPA structures were nanofabricated at the Oak Ridge National Laboratory. Low-resistivity (0.001-0.005 Ω•cm) boron doped p-type ‹100› silicon wafers were spin-coated with ZEP520A resist. Rectangular packed patterns for cylindrical NAPA with P = 337 nm and D = 150 nm were produced by e-beam lithography (JEOL JBX-9300). A 10-nm chromium layer was deposited onto the wafer. Removal of the underlying resist pattern via sonication in acetone left a chromium mask pattern on the substrate. Nanoposts with H = 1200 nm were produced by reactive ion etching using an Oxford PlasmaLab 100 RIE system (the inset in Fig. 1b shows an SEM image of part of an array).

Optimized NAPA have post diameters and heights of D = 150 nm and H = 1200 nm, respectively with a periodicity of P = 337 nm. Ion yields from NAPA structures exhibit strong polarization dependence. When a plane-polarized laser beam impinges on a NAPA, the p component of the electric field vector, $\mathbf{E_p}$, induces a current, **J**, in the posts, resulting in energy dissipation (see Fig. S1) and efficient ion production. The yield of ions produced from adsorbates drops rapidly as the plane of polarization is rotated away from p-polarized and reaches zero as s-polarized irradiation is approached. Desorption of the adsorbates is thought to be induced by the rapid heating of the posts due to the deposition and radial confinement of laser energy, whereas ionization is facilitated by strong near-field

enhancement of the electromagnetic radiation around the posts and the confinement of the laser-induced plume in the troughs between the posts.

Yeast were grown in an incubator shaker using 10 mL water, 2.5 mL 100 g/L D(+) glucose, 0.25 g peptone, and 0.125 g yeast extract (all biochemicals came from Sigma-Aldrich) and cultured for 48 hours at 23 °C. Oxidative stress was induced by exposing cell populations to 1 mM hydrogen peroxide (Sigma-Aldrich) for one hour. Small cell populations were deposited onto NAPA surfaces and allowed to dry before analysis. Population sizes were determined using an optical microscope (BX 51, Olympus) with long working distance objectives.

Yeast cells deposited on NAPA were analyzed by LDI-MS in a Kratos Axima CFR mass spectrometer using 337-nm laser radiation. The list of detected yeast metabolites and major biochemical pathways were assigned using the Saccharomyces Genome Database (SGD).

Materials. Yeast extract, peptone, D-(+)-glucose solution (10%), yeast *Saccharomyces cerevisiae* type II, HPLC grade water, L-methionine, L-cysteine, L-proline, L-lysine, and 50 wt. % hydrogen peroxide solution were purchased from Sigma Chemical Co. (St. Louis, MO). 2,5-dihydroxybenzoic acid was obtained from Protea Biosciences Inc. (Morgantown, WV). Single-side polished mechanical grade, low resistivity (0.001-0.005 Ω•cm) p-type silicon wafers, Si:B ‹100›, 280±20 μm thickness were purchased from University Wafer (South Boston, MA).

Nanopost array fabrication. Nanopost arrays (NAPA) were produced in the clean room of the Center for Nanophase Materials Sciences (CNMS) at the Oak Ridge National Laboratory (Oak Ridge, TN). Low-resistivity p-type silicon wafers were spin-coated with ZEP520A resist at 6000 rpm for 45 seconds and then baked at 180 °C for 2 minutes. Square patterns for the cylindrical posts were produced with periodicities of 337 nm and diameters of 150 nm by e-beam lithography (JEOL JBX-9300). Wafers were soaked in xylenes for 30 seconds to remove the exposed resist and rinsed in isopropanol and blow dried with nitrogen gas. Wafers were then descummed with a Technics reactive ion etching (RIE) system in oxygen plasma at 100 W for 6 seconds. A 10 nm chromium layer was deposited onto the surface with an electron beam evaporator at a rate of 0.1 nm per second. The unexposed resist was dissolved to remove the corresponding chromium layer by sonication of the wafer in an acetone bath for 2.5 minutes. Using RIE in C_4F_8 and SF_6 gases, 1200 nm-high posts were produced at a rate of ~100 nm per minute by an Oxford PlasmaLab 100 RIE system. Scanning electron microscope (SEM) images were captured using an FEI Nova Nanolab 600 DualBeam system.

Culturing of *Saccharomyces cerevisiae*. Medium was created by combining 10 ml of HPLC gradient water, 2.5 ml of glucose solution (100 g/L), 0.25 g peptone, and 0.125 g yeast extract in a 50 ml beaker. Then 0.26 g *Saccharomyces cerevisiae* (Type II from Sigma) was added to the medium and the beaker was covered with Parafilm. In a MaxQ* 4000 refrigerated shaker (Thermo Scientific, Waltham, MA) the

cells were cultured at 150 rpm and 30 °C for 48 hours. For oxidative stress studies 1 mM H_2O_2 was introduced into the culture for 1 hour.

Sample preparation. Aliquots of the resulting yeast population were inspected by an inverted optical microscope (IX 71, Olympus America Corp., Center Valley, PA) to determine the microorganism concentrations. Dilutions were made with HPLC grade water to achieve concentrations that yielded the desired number of cells on the NAPA. After depositing 0.5 μL of the diluted culture, it was allowed to air dry and an optical microscope (BX 51, Olympus) was used to verify the number of cells.

Single cell preparation. The preparation of single yeast cells was initially conducted in a similar manner to larger cell populations. To improve the deposition accuracy and to eliminate liquid overflow on the NAPA platform, a nanospray emitter (SilicaTip, New Objective, Woburn, MA) with 10±1 μm tip diameter was mounted on a translation stage and a syringe pump (SP100I, WPI, Aston, UK) was used to deliver the diluted yeast culture. A partial droplet from the emitter tip was transferred to the NAPA by making contact with its surface and retracting the emitter. Optical microscopy was then used to verify that only a single cell was deposited. The remaining sample volume for a single yeast cell was ~30 fL.

Mass spectrometry. LDI-MS experiments were conducted using an Axima CFR curved field reflectron time-of-flight mass spectrometer (Shimadzu-Kratos, Manchester, UK). Ion generation was achieved by a nitrogen laser emitting 4 ns pulses at 337 nm wavelength focused to a ~200 μm spot size. All mass spectra were the average of 100 laser shots acquired in linear mode. In this regime, the mass resolution of the instrument for the studied mass range below 1,000 Da was $m/\Delta m \approx 3{,}000$. Mass accuracies were better than ~60 mDa. At the typical laser powers used in these experiments, background ions in the absence of cells were negligible. In addition to the LDI-MS experiments, electrospray ionization MS (ESI-MS) was used to help with the identification of the detected compounds. Using a Q-TOF Premier mass spectrometer (Waters Co., Milford, MA, USA) with an electrospray source, we were able to achieve higher mass resolution ($m/\Delta m > 6{,}000$) and better mass accuracy (~5 mDa) than with the LDI-MS system, and had the opportunity to perform tandem MS investigations. Tapping mode atomic force microscopy (AFM) was used (MPP-11100, Veeco, Camarillo, CA) with a high aspect ratio (~17.5° side angle) and small radius (< 10 nm) tip to verify that the cell walls ruptured due to the laser irradiation.

Metabolite identification. The identity of several detected ionic species in the LDI-MS spectra from NAPA was carefully scrutinized. Yeast samples from the control culture were run on the ESI mass spectrometer and in the resulting spectra cytosine, proline, cysteine, homoserine, threonine, lysine, serine, and methionine were identified using accurate mass measurements and isotope distribution patterns. Distinct fragmentation patterns for proline, lysine, methionine, and cysteine were also used to verify their identities. In addition, in the LDI-MS experiments internal standards of proline, lysine, methionine, cysteine, indole, indoleacetaldehyde, dihydroneopterin phosphate, and dihydroneopterin triphosphate

were added to help with the quantitation. The peaks from these internal standards corresponded to the peaks assigned in the yeast spectra.

Quantitation. Quantitative response was established by depositing various amounts of proline, lysine, methionine, and cysteine on NAPA chips and measuring the corresponding ion abundances in LDI-MS experiments. Linear regression for the corresponding calibration curves for lysine and cysteine exhibit correlation coefficients of r = 0.997 and r = 0.983, respectively (see Figure S6). The ion signal was proportional to the deposited amounts of lysine and cysteine covering over four orders of magnitude with the limits of detection (0.3 fmol and 0.8 fmol, respectively) corresponding to quantities below what is estimated to be present in a single yeast cell (20 fmol and 3 fmol, respectively).

Data analysis. Accurate ion masses from the mass spectra were matched with metabolites from the *Saccharomyces* Genome Database (SGD) at http://www.yeastgenome.org/. Pathways were identified using the same database. Peak areas in the spectra were determined using a scientific visualization package (Origin 8.5, OriginLab Corporation, Northampton, MA). Multivariate statistical analyses, i.e., principle component analysis (PCA) and orthogonal projections to latent structures discriminant analysis (OPLS-DA) were conducted by the Extended Statistics (XS) module within the MarkerLynx application manager (Waters Corp., Milford, MA). To identify up- and downregulated metabolites in oxidative stress and to explore cellular differences, the spectra were analyzed using OPLS-DA with Pareto scaling. To verify that the means of the ion intensity distributions for the stressed and control populations were statistically different, paired-sample t-tests were conducted by the Origin 8.5 program.

Supporting Figures

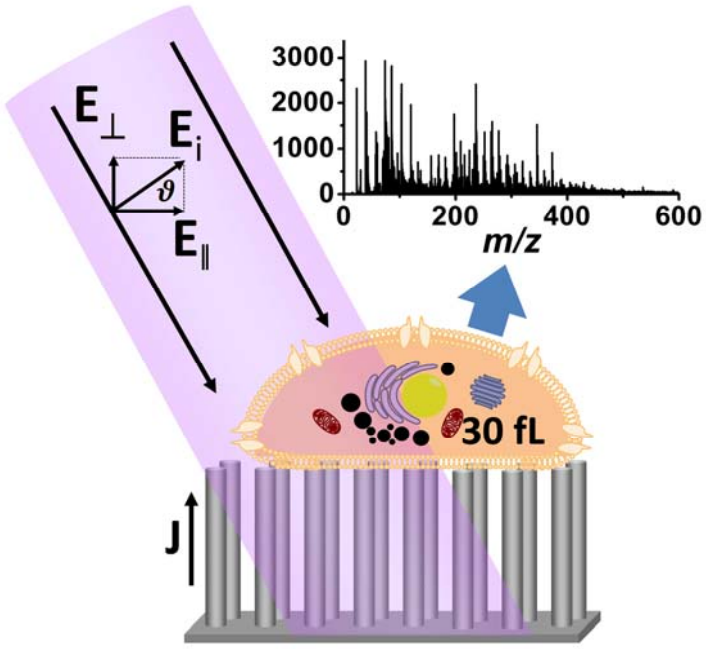

Figure S1. The LDI-MS analysis of small populations and single cells of *S. cerevisiae* on NAPA relies on nanophotonic ion production. The electric field vector, $\mathbf{E_i}$, of the incident p-polarized laser beam induces a current, **J**, in the posts through its $E_\perp = E_i \sin \vartheta$ component, where ϑ is the angle of incidence. A yeast cell of ~30 fL in volume is deposited on the nanoposts. Laser excitation of the posts ruptures the cell, ionizes the metabolites and a mass spectrum can be recorded.

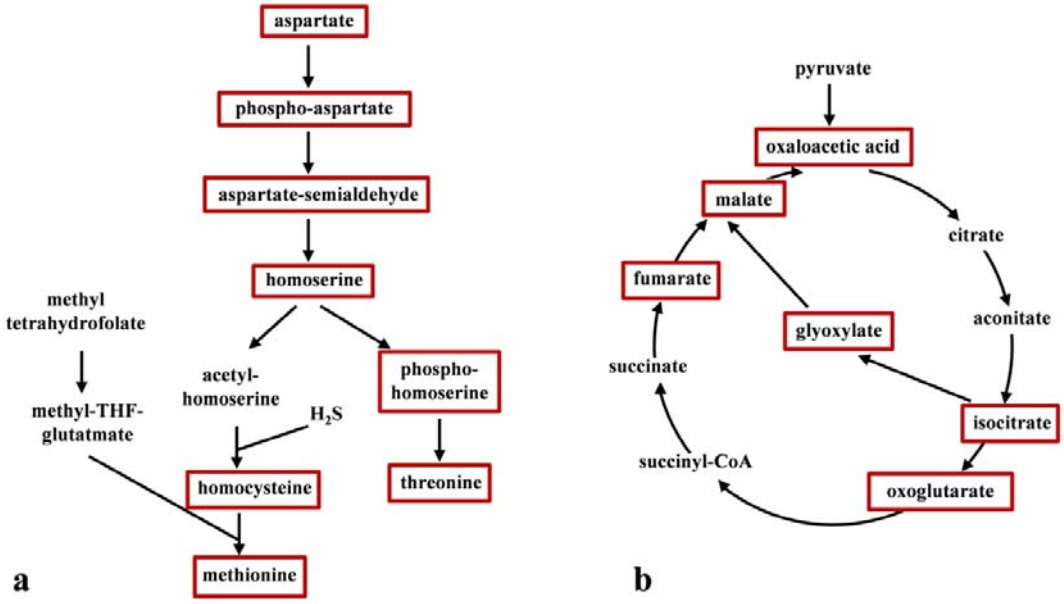

Figure S2. Coverage of selected major biochemical pathways. Selected biochemical pathways that illustrate the metabolite coverage by LDI-MS from NAPA. (a) Superpathway for threonine and methionine biosynthesis and (b) superpathway of tricarboxylic acid (TCA) cycle and glyoxylate cycle. Assigned metabolites are indicated by red frame.

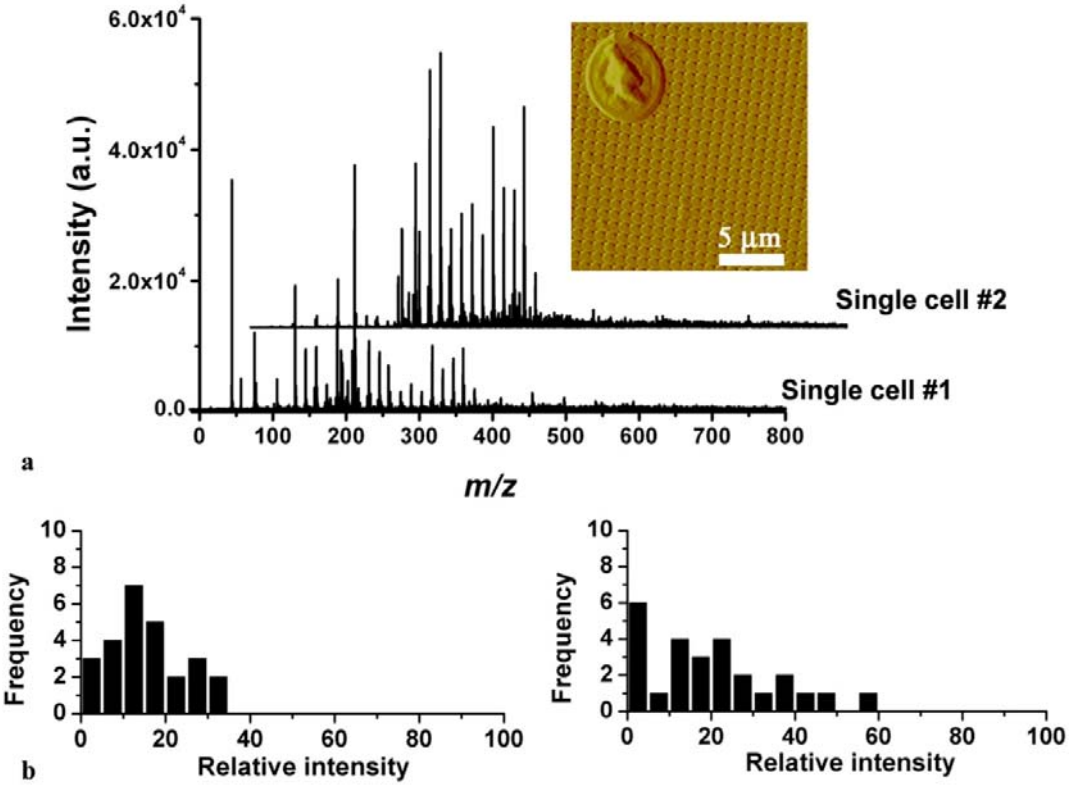

Figure S3. LDI-MS of *S. cerevisiae* from NAPA. (a) LDI mass spectra from individual yeast cells deposited on NAPA. Inset shows the AFM image of a yeast cell on NAPA before analysis. A detailed list of the detected metabolites can be found in B. N. Walker, J. A. Stolee and A. Vertes, *Anal. Chem.* **2012**, *84*, 7756-7762. (b) Ion intensity histograms from single cell mass spectra of (left) leucine and (right) serine based on the analysis of 20 cells.

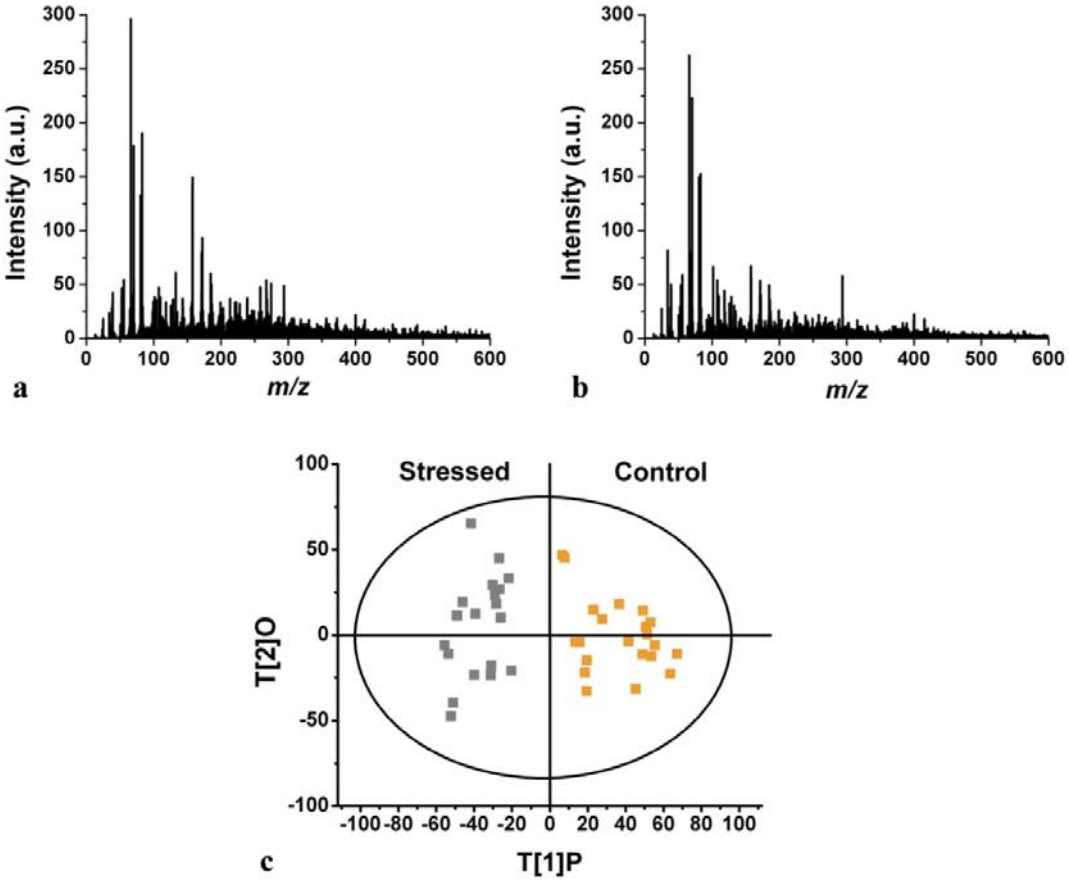

Figure S4. Changes in the mass spectra of single yeast cells reflect the presence of oxidative stress. Single cell LDI mass spectra from NAPA (a) with and (b) without oxidative stress. (c) The OPLS-DA score plot indicates a clear separation of the stressed (gray squares) and control (orange squares) cell spectra. All points are within the 95% Hotelling T^2 ellipse indicating that there are no strong outliers.

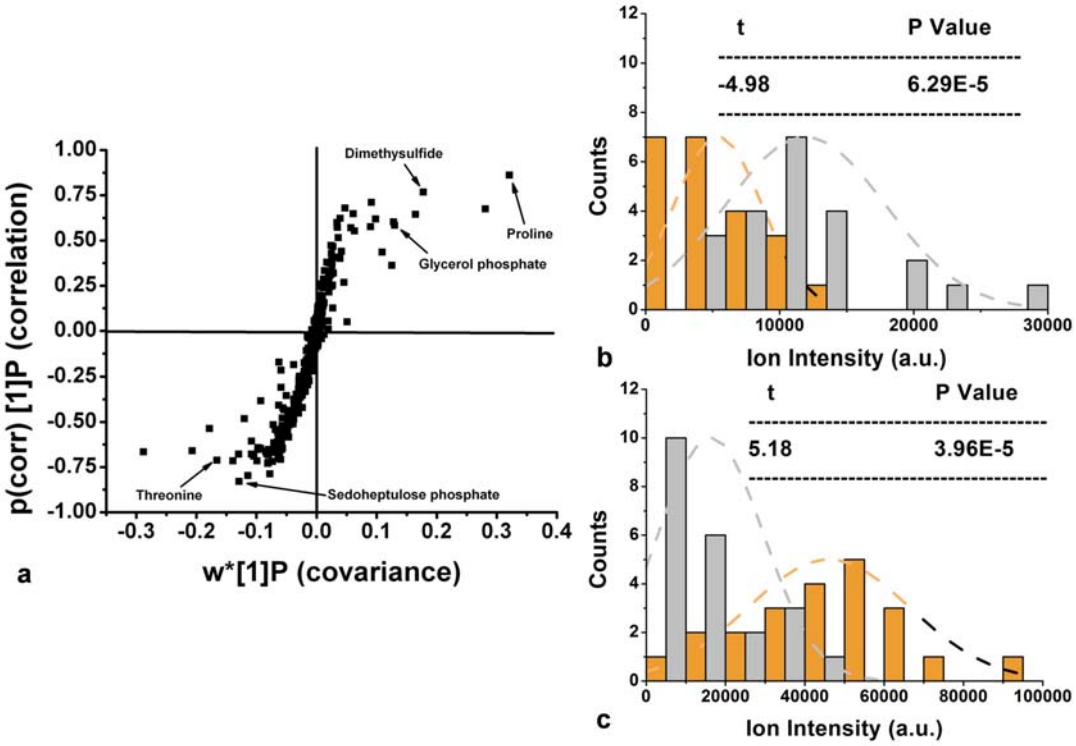

Figure S5. a) Correlation as a function of covariance in the mass spectra yields an S-plot. Metabolites corresponding to the points with high correlation and covariance (the "wings" of the curve) are responsible for most of the variance between the spectra of stressed and control cells. For b) threonine and c) dimethylsulfide histograms of the ion intensity distributions for the stressed (gray bars) and control cells (orange bars) indicate up- and downregulation, respectively. Statistical significance is verified by paired-sample t-tests.

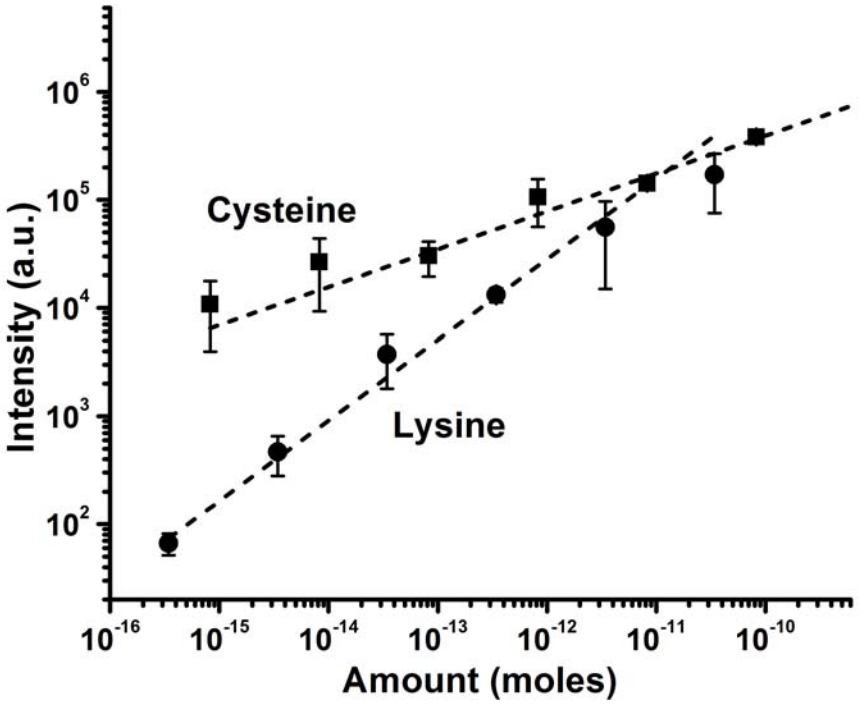

Figure S6. Analysis of lysine and cysteine standards with LDI-MS from NAPA showed that the ion signal was proportional to the deposited amounts for over four orders of magnitude with limits of detection of 0.3 fmol and 0.8 fmol, respectively.

Supporting Tables

Table S1. Tentative assignments of yeast metabolites observed in small cell populations (n ≤ 80) by positive and negative ion LDI-MS from NAPA.** Calculated *m/z* values are based on monoisotopic masses.

#	Assigned metabolite	Ion	Calculated *m/z*	Measured *m/z*	Δ *m/z*
1	Formic acid	$[M+Na]^+$	68.995	68.950	0.045
2	Propionate	$[M-H]^-$	73.030	73.019	0.011
3	Aminoacetone	$[M+H]^+$	74.060	74.050	0.010
		$[M+Na]^+$	96.042	96.012	0.030
4	Amino-propanol	$[M-H]^-$	74.061	74.048	0.013
		$[M+Na]^+$	98.058	98.042	0.016
		$[M+K]^+$	114.081	114.089	-0.008
5	Glyoxylic acid	$[M+H]^+$	75.008	74.994	0.014
		$[M+Na]^+$	96.990	97.010	-0.020
6	Glycine	$[M+H]^+$	76.039	76.047	-0.008
7	Pyrimidine	$[M+H]^+$	81.045	81.010	0.035
8	Thiocyanic acid	$[M+Na]^+$	81.973	81.960	0.013
9	Dimethylsulfide*	$[M+Na]^+$	85.030	85.010	0.020
10	Diacetyl	$[M-H]^-$	85.030	85.039	-0.009
11	Isobutrate	$[M-H]^-$	87.040	87.033	0.007
12	Methanethiol	$[M+K]^+$	87.102	87.064	0.038
13	Putrescine	$[M+H]^+$	89.108	89.064	0.044
14	Glyceraldehyde	$[M+H]^+$	91.039	91.010	0.029
15	Succinic acid-semialdehyde	$[M-H]^-$	101.020	101.040	-0.020
16	Serine	$[M-H]^-$	104.030	104.030	0.000
		$[M+H]^+$	106.051	106.025	0.026
17	Cadaverine	$[M+H]^+$	103.136	103.132	0.004
18	Acetoin	$[M+Na]^+$	111.040	111.000	0.040
19	Cytosine	$[M+H]^+$	112.051	112.054	-0.003
		$[M+K]^+$	150.006	150.000	0.006
20	Uracil	$[M+H]^+$	113.035	113.030	0.005
21	Trimethyl sulfonium	$[M+K]^+$	116.006	115.970	0.036
22	Proline*	$[M+H]^+$	116.053	116.071	-0.018
	Prolinate	$[M-H]^-$	114.050	113.990	0.060
23	Fumaric acid	$[M+H]^+$	117.019	117.010	0.009
		$[M-H]^-$	115.004	115.030	-0.026
24	Aspartate-semialdehyde	$[M+H]^+$	118.050	117.990	0.060
25	Homoserine	$[M-H]^-$	118.050	118.020	0.030
		$[M+H]^+$	120.066	120.025	0.041
26	Threonine	$[M-H]^-$	118.050	118.020	0.030
		$[M+K]^+$	158.060	158.021	0.039
27	Cysteine	$[M-H]^-$	120.012	120.010	0.002
28	Agmatine	$[M-H]^-$	129.110	129.160	-0.050
29	Oxaloacetate	$[M-H]^-$	131.000	131.020	-0.020
30	Glutarate	$[M-H]^-$	131.030	131.020	0.010
31	Aceto-lactate	$[M-H]^-$	131.035	131.020	0.015
32	Asparagine	$[M-H]^-$	131.050	131.020	0.030
33	Glutamic-semialdehyde	$[M+H]^+$	132.066	132.030	0.036
34	Hydroxyproline	$[M+H]^+$	132.103	132.065	0.038
35	Malate	$[M-H]^-$	133.014	133.050	-0.036
36	Acetolactic acid	$[M+H]^+$	133.050	133.074	-0.024
37	Dihydroxy-isovalerate	$[M-H]^-$	133.050	133.050	0.000
38	Deoxyribose	$[M-H]^-$	133.050	133.050	0.000

39	Asparagine	$[M+H]^+$	133.061	133.074	-0.013
40	Ornithine	$[M+H]^+$	133.097	133.074	0.023
		$[M+Na]^+$	155.079	155.074	0.005
41	Aminobenzoic acid	$[M+H]^+$	138.055	138.054	0.001
42	Oxoglutarate	$[M-H]^-$	145.014	145.029	-0.015
43	Glutamine	$[M+H]^+$	147.076	147.073	0.013
44	Methionine	$[M-H]^-$	148.040	148.070	-0.030
45	Xanthine	$[M-H]^-$	151.026	151.050	-0.024
46	Indole	$[M+K]^+$	156.021	156.050	-0.029
47	Orotic acid	$[M+H]^+$	157.024	157.044	-0.020
48	Adenine	$[M+Na]^+$	158.060	158.044	0.016
49	Indoleacetaldehyde	$[M-H]^-$	158.060	158.070	-0.010
		$[M+K]^+$	198.032	198.010	0.022
50	Aminoadipic acid	$[M+H]^+$	162.076	162.054	0.022
51	Phenylalanine	$[M+H]^+$	166.087	166.080	0.007
52	Pyridinedicarboxylate	$[M-H]^-$	166.015	166.028	-0.013
53	Pyridoxamine	$[M+H]^+$	169.097	169.081	0.016
54	Tetrahydrodipicolinate	$[M-H]^-$	170.050	170.050	0.000
55	Glyceraldehyde phosphatidic acid	$[M+H]^+$	171.005	170.969	0.036
56	Dihydroxy-acetone phosphatidic acid	$[M+H]^+$	171.005	170.996	0.009
57	Aspartic acid	$[M+H]^+$	172.072	172.091	-0.019
58	Pyrophosphate	$[M-H]^-$	172.900	172.920	-0.020
		$[M+K]^+$	217.042	217.043	-0.001
59	Glycerol phosphatidic acid*	$[M+H]^+$	173.033	173.021	0.022
60	Homocysteine	$[M+K]^+$	173.999	173.980	0.019
61	Cysteinylglycine	$[M+H]^+$	179.048	179.041	0.007
62	Acetylphosphatidic acid	$[M+K]^+$	178.951	178.950	0.001
63	Histidinol*	$[M+K]^+$	180.037	180.052	-0.015
64	Iditol	$[M+H]^+$	183.086	183.097	-0.011
65	Keto-acetamidocaproate	$[M-H]^-$	186.077	186.100	-0.023
		$[M+K]^+$	226.047	226.062	-0.015
66	Acetyl-glutamate	$[M-H]^-$	188.056	188.050	0.006
67	Isocitrate	$[M-H]^-$	191.020	191.009	0.011
68	Histidine	$[M+K]^+$	194.168	194.163	0.005
69	Gluconate	$[M-H]^-$	195.051	195.049	0.002
70	Phospho-homoserine	$[M+H]^+$	200.030	200.060	-0.030
71	Homocitrate	$[M-H]^-$	205.150	205.140	0.010
72	Lipoamide	$[M+H]^+$	206.067	206.093	-0.026
73	Kynurenine	$[M+H]^+$	208.984	208.991	-0.007
		$[M+Na]^+$	231.074	231.048	0.026
74	Gluconolactone	$[M+K]^+$	217.011	217.006	0.005
75	Pantothenate	$[M-H]^-$	218.103	218.122	-0.019
		$[M+Na]^+$	242.100	242.040	0.060
		$[M+K]^+$	258.074	258.130	-0.056
76	Tyrosine	$[M+K]^+$	220.037	220.020	0.017
77	Aminodeoxychorismic acid	$[M+H]^+$	226.068	226.077	-0.009
78	Chorismic acid	$[M+H]^+$	227.056	227.080	-0.024
79	Deoxycytidine	$[M+H]^+$	228.098	228.070	0.028
80	Xylulose phosphatidic acid	$[M+H]^+$	231.027	231.048	-0.021
81	Cytidine	$[M+H]^+$	244.093	244.040	0.053
		$[M+K]^+$	282.049	282.060	-0.011
82	Pyridoxal phosphatidic acid	$[M+H]^+$	248.032	248.010	0.022

		$[M+Na]^+$	270.014	270.060	-0.046
		$[M+K]^+$	285.988	286.020	-0.032
83	Glucosamine phosphatidic acid	$[M+H]^+$	260.053	260.049	0.004
84	Glutamate phosphatidic acid	$[M+K]^+$	265.983	265.990	-0.007
85	Inosine	$[M-H]^-$	267.070	267.090	-0.020
		$[M+H]^+$	269.088	269.070	0.018
		$[M+K]^+$	307.044	307.072	-0.028
86	Adenosine	$[M+H]^+$	268.104	268.080	0.024
87	Naringenin	$[M-H]^-$	271.061	271.023	0.038
88	Pyridoxine phosphatidic acid	$[M+Na]^+$	272.029	272.010	0.019
		$[M+K]^+$	288.003	288.030	-0.027
89	Xanthosine	$[M-H]^-$	283.068	283.032	0.036
		$[M+K]^+$	323.039	323.032	0.007
90	Sedoheptulose phosphatidic acid*	$[M+H]^+$	290.160	290.101	0.059
91	Methylthioadenosine	$[M+H]^+$	298.052	298.040	0.012
92	Acetyl-glucosamine phosphatidic acid	$[M+H]^+$	302.063	302.040	0.023
		$[M+K]^+$	340.019	340.010	0.009
93	Thiamine	$[M+K]^+$	304.075	304.048	0.027
94	Deoxycytidine monophosphate	$[M-H]^-$	306.050	306.070	-0.020
95	Glutathione	$[M-H]^-$	306.080	306.070	0.010
		$[M+H]^+$	308.091	308.073	0.018
96	Succinyl-amino-ketopimelic acid	$[M+Na]^+$	312.069	312.040	0.029
		$[M+K]^+$	328.043	328.060	-0.017
97	Phosphoribosyl-formylglycineamide	$[M+H]^+$	314.075	314.070	0.005
		$[M-H]^-$	312.060	312.081	-0.021
98	Phytosphingosine	$[M+H]^+$	318.300	318.312	-0.012
99	Dihydroneopterin phosphatidic acid	$[M+H]^+$	336.128	336.113	0.015
100	Adenosylmethioninamine	$[M-H]^-$	354.150	354.120	0.030
101	Thymidine diphosphatidic acid	$[M+H]^+$	403.030	403.042	-0.012
102	Deoxyuridine diphosphatidic acid	$[M+Na]^+$	411.420	411.391	0.029
103	Phosphatidyl-myo-inositol	$[M+Na]^+$	413.046	413.010	0.036
		$[M+K]^+$	429.020	429.020	0.000
104	Dihydrofolic acid	$[M+H]^+$	444.163	444.149	0.014
105	Tetrahydrofolic acid	$[M+H]^+$	446.178	446.183	-0.005
		$[M+Na]^+$	468.160	468.141	0.019
106	Riboflavin phosphate	$[M-H]^-$	457.110	457.120	-0.010
107	Dihydroneopterin triphosphate	$[M-H]^-$	493.990	493.990	0.000
108	Guanosine triphosphatidic acid	$[M+Na]^+$	545.980	545.962	0.018

*Metabolite ions observed only in the single cell studies.

Experience with NAPA ionization indicates that the ratio of the H^+, Na^+ and K^+ adducts changes with the applied laser power. At low laser powers, the H^+ adduct is prominent. As the laser power is increased Na^+ adducts become more abundant. Further increasing the laser power results in the dominance of the K^+ adducts. The crossover from one adduct type to another depends, in part, on the nature of the ionized molecule. Thus, it is possible that, at the power used for these experiments, the different metabolites are primarily present in different ionic forms. Our related results for the case of three peptides have been reported in the literature: B. N. Walker, J. A. Stolee, D. L. Pickel, S. T. Retterer, A. Vertes, *Appl. Phys. A* **2010, *101*, 539-544.

Table S2. Aggregated metabolite coverage for families of yeast biochemical pathways and super-pathways using LDI-MS from NAPA. Labels in the first column correspond to the labels in Figure 1c. The percentages are calculated with the assumption that all the tentative assignments in Table 1 are correct.

Label	Pathway family	Assigned metabolites (%)
A	Amino acid biosynthesis	22.4
B	Fatty acid and lipid biosynthesis	4.3
C	Carbohydrate biosynthesis	6.8
D	Nucleoside and nucleotide biosynthesis	21.5
E	Cofactor, prosthetic group, and electron carrier biosynthesis	24.3
F	Amino acid degradation	40.4
G	Carbohydrate degradation	0.0
H	All other biochemical pathways	12.0

Table S3. Up- and downregulated metabolites in oxidative stress of yeast.** The data for the first 21 metabolites stemming from small population studies (n ≈ 80) is depicted in Figure 3 of the main text. The intensity ratios $I_S/I_C > 1$ and $I_C/I_S > 1$ for each metabolite gauge the degree of up- and downregulation, respectively. Here I_C and I_S stand for the intensity of an ion in the control and stressed populations, respectively. In case of ambiguous assignments the most likely isomers are listed. Calculated *m/z* values are based on monoisotopic masses.

#	Assigned metabolite	Ion	Calculated *m/z*	Measured *m/z*	Δ *m/z*	I_S/I_C	I_C/I_S	p-value
1	Ethanolamine	$[M+H]^+$	62.061	62.013	0.048		5.34	2×10^{-4}
2	Alanine	$[M+H]^+$	90.050	90.000	0.050		1.70	3×10^{-5}
3	Oxoproline	$[M+H]^+$	130.000	129.958	0.042		11.49	3×10^{-4}
4	Benzaldehyde	$[M+K]^+$	145.140	145.142	-0.002		4.53	2×10^{-3}
5	Cumic-aldehyde	$[M+Na]^+$	171.079	171.072	0.007		6.32	1×10^{-6}
	Dihydroxy methylvaleric acid	$[M+Na]^+$	171.063	171.072	-0.009		6.32	1×10^{-6}
	Mevalonic acid	$[M+Na]^+$	171.063	171.072	-0.009		6.32	1×10^{-6}
	Oxalureate	$[M+K]^+$	171.115	171.072	0.043		6.32	1×10^{-6}
6	Tetrahydrodipicolinic acid	$[M+H]^+$	172.061	172.087	-0.026		2.49	7×10^{-3}
	Methionine	$[M+Na]^+$	172.041	172.087	-0.046		2.49	7×10^{-3}
	Aspartic acid	$[M+K]^+$	172.136	172.087	0.049		2.49	7×10^{-3}
7	Tyrosol	$[M+K]^+$	177.166	177.168	-0.002	2.28		2×10^{-4}
8	Cysteinylglycine	$[M+H]^+$	178.210	178.202	0.008	1.93		1×10^{-2}
9	Acetyl-lysine	$[M+H]^+$	189.159	189.153	0.006	2.58		6×10^{-3}
10	Dehydroquinic acid	$[M+H]^+$	191.056	191.058	-0.002	2.38		3×10^{-4}
	Pyridoxamine	$[M+Na]^+$	191.080	191.058	0.022	2.38		3×10^{-4}
	Uric acid	$[M+Na]^+$	191.018	191.058	-0.040	2.38		3×10^{-4}
11	Erythrose phosphatidic acid	$[M+H]^+$	201.080	201.120	-0.040	12.60		1×10^{-7}
12	Glutamylcysteine	$[M+H]^+$	251.270	251.304	-0.034	4.70		3×10^{-6}
13	Phospho-gluco-lactone	$[M+H]^+$	258.120	258.116	0.004	5.88		2×10^{-3}
14	Glucose phosphatidic acid	$[M+H]^+$	260.120	260.097	0.023	15.13		4×10^{-6}
	Fructose phosphatidic acid	$[M+H]^+$	260.120	260.097	0.023	15.13		4×10^{-6}
15	Amino deoxychorismic acid	$[M+H]^+$	264.162	264.113	0.049		2.85	4×10^{-4}
16	Sedoheptulose phosphatidic acid	$[M+H]^+$	290.160	290.101	0.059	4.68		1×10^{-2}
17	Glutathione	$[M+H]^+$	307.320	307.310	0.010	3.43		2×10^{-3}
18	Cytidine phosphatidic acid	$[M+H]^+$	324.060	324.041	0.019	2.30		4×10^{-3}
19	Dihydroneopterin phosphatidic acid	$[M+Na]^+$	358.053	358.029	0.024		2.84	2×10^{-6}
	Formylglutathione	$[M+Na]^+$	358.068	358.029	0.039		2.84	2×10^{-6}
20	Dihydroxyicosa-tetraenoic acid	$[M+K]^+$	375.328	375.342	-0.014		6.92	3×10^{-3}
21	Guanosine triphosphatidic acid	$[M+Na]^+$	545.980	545.962	0.018	3.82		4×10^{-2}
22	Dimethylsulfide*	$[M+Na]^+$	85.037	85.013	0.024		6.24	4×10^{-6}
23	Proline*	$[M+H]^+$	116.053	116.071	-0.018		7.13	7×10^{-6}
24	Threonine*	$[M+K]^+$	158.052	158.021	0.031	5.22		6×10^{-5}
25	Glycerol phosphatidic acid*	$[M+H]^+$	173.036	173.022	0.014		7.23	3×10^{-5}
26	Histidinol*	$[M+K]^+$	180.037	180.052	-0.015		2.35	2×10^{-3}

*Metabolite ion intensity changes observed only in the single cell studies.

Experience with NAPA ionization indicates that the ratio of the H^+, Na^+ and K^+ adducts changes with the applied laser power. At low laser powers, the H^+ adduct is prominent. As the laser power is increased Na^+ adducts become more abundant. Further increasing the laser power results in the dominance of the K^+ adducts. The crossover from one adduct type to another depends, in part, on the nature of the ionized molecule. Thus, it is possible that, at the power used for these experiments, the different metabolites are primarily present in different ionic forms. Our related results for the case of three peptides have been reported in the literature: B. N. Walker, J. A. Stolee, D. L. Pickel, S. T. Retterer, A. Vertes, *Appl. Phys. A* **2010, *101*, 539-544.